In vitro antibiofilm activity-directed in silico identification of natural products targeting bacterial biofilm regulators SarA and LasR

Jamil A Shilpi[1*], Dipto Kumer Sarker[1], Veronique Seidel[2], Mohammad Tuhin Ali[3], Shaikh Jamal Uddin[1], Ananya Basak[1], Shaown Chakraborty[1], M Khairuzzaman[1], Akhlak Un Nahar[1], Fayad Bin Abdus Salam[1]

[1]Pharmacy Discipline, Life Science School, Khulna University, Khulna 9208, Bangladesh

[2]Natural Products Research Laboratory, Strathclyde Institute of Pharmacy and Biomedical Sciences, University of Strathclyde, Glasgow, UK

[3]Department of Biochemistry and Molecular Biology, University of Dhaka, Dhaka 1000, Bangladesh

ORCID author IDs:
Jamil A Shilpi: 0000-0001-8938-9240
Dipto Kumer Sarker: 0000-0002-6033-9669
Veronique Seidel: 0000-0003-3880-5261
Mohammad Tuhin Ali: 0000-0002-0889-6548
Shaikh Jamal Uddin: 0000-0003-3163-2118
M Khairuzzaman: 0000-0001-8269-3450
Fayad Bin Abdus Salam: 0000-0002-1928-7676

***Correspondence**

Jamil A Shilpi

Email: jamilshilpi@pharm.ku.ac.bd

Mobile: +8801910010054

Abstract

Background: Antibiofilm agents serve as an essential tool in the fight against antibiotic resistance, and natural products provide a promising source for potential drug leads.

Objective: This study investigates the activity of twenty Bangladeshi medicinal plants against *Staphylococcus aureus* and *Pseudomonas aeruginosa* biofilms and predicts the interactions of selected phytochemicals from five of the best performing plants with the active sites of transcriptional regulatory proteins SarA of *S. aureus* and LasR of *P. aeruginosa*.

Methods: The plant extracts were tested by microtiter plate-based assay against *S. aureus* and *P. aeruginosa* biofilms. Molecular docking and molecular dynamics simulation (MD) were conducted using PyRx and GROMACS, respectively.

Results: The best activity was identified for *Cassia fistula* and *Ananas comosus*, showing ≥ 75% inhibition of biofilm formation. *ent*-Epicatechin-(4α→8)-epiafzelechin (EEE) of *C. fistula*, cyanidin-3,3',5-tri-*O*-β-D-glucopyranoside (CTG) of *A. comosus*, and 7-*O*-(4-hydroxy-*E*-cinnamoyl)-spinoside of *A. spinosus* showed the best predictive binding affinity (-7.6, -7.6 and -7.7 kcal/mol, respectively) for SarA. EEE was the only ligand to exhibit a stable ligand-protein complex with SarA in the MD simulation of 200 ns (binding energy of MMPBSA analysis -39.899 kJ/mol). Chrysophanol, epicatechin and physcion, of *C. fistula* (-10.5, -10.5, and -11.0 kcal/mol, respectively) and auraptene of *F. limonia* (-10.8 kcal/mol) showed the best predictive binding affinity for LasR. Epicatechin showed the most stable ligand-protein complex with LasR (binding energy of MMPBSA analysis -63.717 kJ/mol).

Conclusion: Epicatechin and its derivative EEE could be used as scaffolds for the development of new antibiofilm agents against *P. aeruginosa* and *S. aureus*, respectively.

Keywords: Antibiofilm; Natural products; *Staphylococcus aureus*; *Pseudomonas aeruginosa*; *Cassia fistula*; Epicatechin.

1. INTRODUCTION

Biofilms are formed when microbes produce an extracellular polymeric matrix, composed mainly of polysaccharides, proteins and nucleic acids, to help them adhere to surfaces [1-2]. This matrix acts as a reservoir for the microbial community to thrive, protected from the host's defence system and from disinfectants or antibiotics [3-4]. Most of the currently available antibiotics are unable to target bacteria residing inside biofilms, resulting in the persistence and recurrence of infection [5]. The exposure of microbes to sub-inhibitory concentrations of some antibiotics also favours biofilm formation, which further exacerbates the problem [6-8]. The formation of microbial biofilms on surfaces and medical devices such as catheters, endoscopes or implants is an important cause of infection in hospital settings [9-10].

Pseudomonas aeruginosa and *Staphylococcus aureus* are common nosocomial pathogens that are able to form biofilms in human tissues and medical devices [11]. In the search for new antibiofilm agents, the SarA protein of *S. aureus* and LasR protein of *P. aeruginosa* have become attractive targets [12-13]. Both are transcriptional activators of bacterial quorum-sensing (QS) that control biofilm formation and the expression of virulence factors. The binding of quorum sensing molecules with these transcriptional regulatory proteins activates the transcription of virulence factors such as exotoxins, exoproteases and secondary metabolites necessary for biofilm formation. SarA is one of the most extensively studied

transcription regulatory protein. It controls 120 genes associated with proteins that influence biofilm formation [14-15]. LasR is a global regulator of virulence genes. It has been established that a lack of LasR function results in QS inactivation and loss of pathogenicity [16-17].

Natural products, including plants and their phytoconstituents, may offer an alternative approach to prevent microbial biofilm formation and/or eradicate biofilms [13, 18-19]. Plants from Bangladesh have a long history of use in traditional medicine, including in the treatment of infection [20]. In this study, we tested the *in vitro* activity of twenty Bangladeshi medicinal plants against *S. aureus* and *P. aeruginosa* biofilms. These plants were selected on the basis of their previously reported antibacterial activity against various pathogens and/or of their use in traditional medicine for the management of infections (Table S1). Such ethnobotanical considerations provide a rational approach for drug discovery purposes since biological activity is often established following a long history of use with success [21-22]. Plants showing the most potent antibiofilm activity were further selected for an *in silico* study. A molecular docking approach was performed to predict the binding affinity of selected phytoconstituents from these plants towards SarA and LasR. The ligands with the highest binding affinities were further checked for the stability of their protein-ligand complexes using molecular dynamics simulations.

2. MATERIALS AND METHODS

2.1. Plant material

Plants, traditionally used for infections and/or previously reported to have antibacterial activity, were collected during July-Oct from different regions of the Khulna district (Bangladesh) (Table S1). Plants were identified by the experts at Bangladesh National Herbarium while

voucher specimen were submitted for five plants, which showed best *in vitro* antibiofilm activity and were chosen for *in silico* studies. Voucher specimen were submitted for *A. spinosus* (DACB 90388), *A. comosus* (DACB 92284), *C. fistula* (DACB 90385), *F. limonia* (DACB 92285) and *T. indica* (DACB 90386). Accepted names of these plants as appears on World Flora Online database were used throughout this manuscript (http://www.worldfloraonline.org/).

2.2. Extraction

The plant materials were washed, shade-dried and ground into coarse powder. The powdered materials were then macerated in ethanol for 3 days with occasional stirring (Table S2). The filtrate was evaporated to dryness under reduced pressure at < 45 °C to afford each crude extract (Table 1). The latter were transferred to glass vials and stored at -20 °C until further analysis.

2.3. Bacterial cultures

Staphylococcus aureus (NCTC 12981) and *Pseudomonas aeruginosa* (NCTC 12903) were obtained from the Microbiology Laboratory of Biotechnology and Genetic Engineering Discipline, Khulna University. Following two sub-cultures on nutrient agar and incubation at 37 °C for 16-18 h, the bacterial inoculum was prepared in sterile 0.9% saline to reach a density of 0.5 McFarland using a Grant-bio DEN-1 McFarland densitometer [23]. Further dilutions were made to achieve a bacterial stock concentration of 5×10^5 CFU/mL for the microbiological assays.

2.4. Chemicals and reagents

Ethanol, nutrient agar, nutrient broth, sulphuric acid and glacial acetic acid were obtained from Merck (India) while resazurin, crystal violet and barium chloride were obtained from Loba Chemie Private Ltd (India). Eugenol and epicatechin were purchased from Tokyo Chemical Industries Company Ltd (Japan). Ciprofloxacin and gentamicin were generously provided by Incepta Pharmaceuticals Ltd (Bangladesh).

2.5. Determination of MIC values

Prior to screening for antibiofilm activity, the minimum inhibitory concentration (MIC) values of all plant extracts were first determined using a broth microdilution assay [24]. Stock solutions of extracts and antibiotic standards were prepared with 5% DMSO in sterile 0.9% saline to achieve concentrations of 2000 and 100 µg/mL, respectively. Serial dilutions were made in 96-well round-bottomed microtitre plates (Sigma-Aldrich, USA) containing nutrient broth to get a starting concentration of 500 µg/mL (extracts) and 25 µg/mL (antibiotics) and a final volume of 100 µL in each well. After addition of the bacterial inoculum (100 µL, 1×10^6 CFU/mL), the microtitre plates were incubated at 37 °C for 24 h. At the end of the incubation period, 5 µL resazurin was added and after 2 h, the MICs were recorded through visual inspection of the colour change of resazurin. The experiments were carried out in duplicate on different days.

2.6. Antibiofilm assay

This assay followed a previously published methodology [25-26]. In this case, after incubation of the microtitre plates at 37 °C for 24 h, the liquid medium containing sessile bacteria was removed before 100 µL of 1% w/v aqueous solution of crystal violet was added. Then, the dye

was removed and the wells were washed with distilled water. For the quantification of biofilm adherence, 125 µL of 30% acetic acid was added to each well and kept for 30 min. The resulting solution was transferred into new flat-bottomed microtitre plates (Sigma-Aldrich, USA) and the absorbance was measured at 570 nm using a microplate reader (Multiskan GO, Thermo Scientific). Eugenol and epicatechin were used as the positive controls [27-28]. The experiments were done in duplicate and the inhibition of biofilm formation was calculated using the following equation where OD stands for optical density.

$$\% \, Inhibition = \frac{OD_{control} - OD_{treatment}}{OD_{control}} \times 100$$

2.7. Molecular docking

2.7.1. Preparation of proteins

The three-dimensional structures of *S. aureus* SarA (PDB ID:2FRH) and *P. aeruginosa* LasR (PDB ID: 2UV0) were downloaded from the Protein Data Bank (https://www.rcsb.org/). The protein structures were prepared for the docking using BIOVIA Discovery Studio Visualizer v.4.5 (DSv.4.5) and AutoDock Tools (v.1.5.7), removing water molecules and co-crystallised ligands, selecting protein chains, adding polar hydrogens and Kollman charges, distributing charges evenly and repairing missing atoms.

2.7.2. Preparation of ligands

The Dictionary of Natural Products (DNP) published by Routledge (Taylor and Francis Group) was consulted to compile all compounds previously reported from the five plant extracts with the most prominent antibiofilm activity (*A. spinosus*, *A. comosus*, *C. fistula*, *F. limonia* and *T.*

indica). The 3D chemical structures of 161 secondary metabolites were downloaded in SDF format from the NCBI PubChem database (https://pubchem.ncbi.nlm.nih.gov/) or drawn using ChemOffice v.21.0.0. The preparation of the ligands, including energy minimisation, was done using the Open Babel module of PyRx (v.0.8) using a universal force field (uff). *N*-3-oxo dodecanoyl-L homoserin lactone (OHN), retrieved from its co-crystallized complex with 2UV0, was used as the control inhibitor for LasR while 2,4-diflurobenzyl)amino]cyclohexanol (SarABI) [29] and ZINC00990144 [30] were used as the control inhibitors for SarA.

2.7.3. Grid box generation and molecular docking

The binding sites of SarA and LasR were identified from previous literature reports [12, 31]. Docking of the ligands at the binding sites of selected proteins were conducted with the Autodock Vina based virtual screening module of PyRx (v.0.8). The centre of the grid box was set to x = 37.5, y = -2.7, z = 20.8 and x = 25.3, y = 38.2, z = 43.2 for SarA and LasR, respectively. Their sizes were 26 × 32 × 31 and 27 × 24 × 23, respectively with the spacing set at 1Å and exhaustiveness set to 8. The docking scores were calculated as the predicted free energies of binding (ΔG in kcal/mol). Ligands were ranked according to their docking scores with RMSD 0 and ligands with best docking scores were checked for their binding pose [32-33]. Discovery Studio v.4.5 and LigPlot+ v.2.2 were used to visualise the specific intermolecular interactions between the best ligand docking poses and the binding sites of the studied proteins.

2.8. Molecular dynamics simulations

GROMACS 2021 was employed to perform molecular dynamics (MD) simulations, using a CHARM36 force field [34-35]. The CHARMM General FF (CGenFF) (https://cgenff.silcsbio.com) server was used for ligand parameterization [36]. The system was then solvated using a TIP3P water model in a cubic box. Further neutralisation was performed by addition of Na^+ and Cl^- ions following energy minimisation. To equilibrate the system, NVT and NPT ensembles for 1 ns were performed at 300 °K and 1 bar. The system was projected for final MD runs for 200 ns of the best docked ligands and control molecules with LasR and SarA. Root means square deviations **(**RMSD), root means square fluctuations (RMSF), radius of gyration (Rg), solvent accessible surface area (SASA) and hydrogen bond analysis were used to analyse the trajectories. The g_mmpbsa tool was used for the Molecular Mechanics Poisson-Boltzmann Surface Area (MMPBSA) analysis of the last 100 ns, and snapshots were taken at the 100 ps time step [37].

2.9. Pharmacokinetics and drug-likeness prediction

Canonical SMILES of selected ligands were retrieved from the PubChem database. The SwissADME online tool (http://www.swissadme.ch/) and OSIRIS property explorer software (https://www.organic-chemistry.org/prog/peo/) were used to obtain the physicochemical descriptors, pharmacokinetic and drug-likeness properties, as well as other important parameters that have to be taken into account before a compound can be considered as a possible drug lead [38].

3. RESULTS

3.1. Determination of MIC values

The best antibacterial activity was observed for *M. longifolium* extract with MICs of 62.5 and 125 µg/mL against *S. aureus* and *P. aeruginosa*, respectively. Both *A. spinosus* and *J. adhatoda* extract showed MICs of 250 µg/mL against *S. aureus* and 62.5 µg/mL against *P. aeruginosa*. The remaining plant extracts exhibited MIC values of either 250 or 500 µg/mL against the test pathogens. Ciprofloxacin and gentamicin showed MICs of 1.56 and 0.78 µg/mL, respectively against both pathogens (Table 1).

3.2. Antibiofilm activity

The percentage inhibition of biofilm formation by the best performing five plant extracts, namely *A. comosus, C. fistula, A. spinosus, F. limonia* and *T. indica* are depicted in Fig. 1 and Fig. 2. The highest inhibition of biofilm formation was observed for *C. fistula* extract against both pathogens with strong inhibition maintained at all the concentrations tested. The rest of the plant extracts showed some degree of antibiofilm activity against the test pathogens (Table S3 and S4). Eugenol and epicatechin, used as standard antibiofilm agents, displayed mild to moderate antibiofilm activity against both test pathogens (Table S3 and S4).

3.3. Molecular docking

Docking score of all the phytoconstituents against SarA and LasR proteins are listed in Table S7. Among all the ligands, 7-*O*-(4-Hydroxy-*E*-cinnamoyl)-spinoside (HCS) (-7.7 kcal/mol) from *A. spinosus*, 14-dihydroxycard-20(22)-enolide-xylopyranosyl (-7.7 kcal/mol) from *T. indica*, cyanidin-3,3',5-tri-*O*-β-D-glucopyranoside (CTG) (-7.6 kcal/mol) from *A. comosus*, and *ent*-epicatechin-(4α→8)-epiafzelechin (2*S*,2'*R*,3*S*,3'*R*,4β form) (EEE) (-7.6 kcal/mol) from

C. fistula showed the highest binding affinity for SarA, with scores above that of the control inhibitor SarABI (-5.8) and similar to that of ZINC00990144 (-7.9) (Table 2). Physcion (-11.0 kcal/mol), epicatechin (-10.5 kcal/mol) and chrysophanol (-10.5 kcal/mol) from *C. fistula* as well as auraptene (-10.8 kcal/mol) from *F. limonia*, showed the highest binding affinity for LasR, with scores above that of the control OHN (-9.0 kcal/mol) (Table 3). Eugenol, used as a control in our antibiofilm assay, displayed a binding affinity of -4.8 and -6.8 kcal/mol for SarA and LasR, respectively. These phytoconstituents showed interactions with key amino acid residues at the binding site of each protein (Table S5, S6 and Fig. 3, 4, S1-S8). Physcion, auraptene, epicatechin, HCS, CTG, EEE and the control ligands OHN and ZINC00990144 were selected for further molecular dynamics simulations studies.

3.4. Molecular dynamics simulations

3.4.1 RMSD analysis

Among the investigated compounds, the epicatechin-LasR complex showed the highest stable trajectories (mean, 1.9 Å) over the MD simulations. At the beginning of the simulation, this complex showed higher fluctuations that decreased after 24 ns. From 24 ns to 71 ns, it showed a gradual increasing trend with minimal fluctuations (mean, 1.8 Å). From 71 ns to the end of the simulation, this complex fluctuated near a mean of 2.0 Å. In contrast, the physcion-LasR complex showed an initially lower RMSD that became higher, particularly within 28-54 ns, 153-160 ns, and from 179 ns to the end of the study. In addition, this complex showed multiple fluctuations during the simulation period with an overall mean of 2.0 Å. The auraptene-LasR complex showed a comparatively stable RMSD within 20-43 ns, after that the value gradually

253 increased till 162 ns (mean, 2.5 Å). From 163 ns onwards, the fluctuations decreased steadily
254 until the end of the simulation, with a mean fluctuation of 2.5 Å. The OHN-LasR complex
255 fluctuated highly during the initial 50 ns and stabilised after 50 ns (Fig. 5a). In addition, this
256 complex showed higher stability, compared to the epicatechin-LasR complex, during the last
257 65 ns of the study.
258 Unlike CTG, HCS and ZINC00990144 which left the binding site of SarA, EEE was found to
259 bind effectively to this protein and was therefore the only ligand considered for further MD
260 analysis. The apo protein showed high fluctuations before 89 ns and stabilised after 121 ns
261 (Fig. 7a). By contrast, the EEE-SarA complex showed high fluctuations initially and achieved
262 convergence between 39-54 ns of the study. After 55 ns and until the end of the study, no
263 noticeable abrupt fluctuations were noticed, and fluctuations near a mean of 4.5 Å suggested
264 higher stability and lower structural deviations.
265
266 ***3.4.2 RMSF analysis***
267 The Cα atoms of the LasR apo protein showed higher fluctuations, notably in the *N* and *C*-
268 terminal, 13–14, 38–50, and 119–125 residues. All ligand-bound proteins exhibited minimal
269 fluctuations compared to the apo protein, and this scenario was noticeable for the epicatechin,
270 auraptene, and OHN-bound proteins, indicating higher stability (Fig. 5b). In addition, the
271 physcion bound protein showed higher fluctuations within 88-98 residues. In the case of SarA,
272 high fluctuations in the N-terminal region were observed for both the apo protein and the EEE-
273 bound protein, although the fluctuations were relatively low for the latter (Fig. 7b). The EEE-
274 bound protein showed high fluctuation in its C-terminal region compared to the apo protein.

Additionally, the EEE-SarA complex showed high fluctuations within residues 182-191, which includes the binding site residues.

3.4.3 Radius of gyration analysis

The Rg for LasR protein-ligand complex with epicatechin, physcion, and OHN showed a stable trajectory within an almost identical mean value of 15.6 Å for each of the protein-ligand complex. On the other hand, the auraptene-LasR also showed a slightly higher mean of 15.7 Å, since it showed higher Rg value from the beginning to 38 ns of the study (Fig. 5c). The apo protein SarA showed a lower mean Rg (16.3 Å) than that of the EEE-protein complex (17.1 Å) (Fig. 7c).

3.4.4 SASA analysis

All LasR-ligand complexes demonstrated similar extent of SASA (90.41, 90.64, 91.37, 92.75 nm^2 for physcion, OHN, epicatechin and auraptene, respectively) (Fig. 5d). The EEE-SarA complex initially showed a high SASA value which decreased after 23 ns. The SASA value for SarA apoprotein was low compared to the EEE-SarA complex (Fig. 7d).

3.4.5 Number of hydrogen bonds

EEE showed the highest number of hydrogen bonds with LasR (1-6) followed by OHN (1-5), physcion (1-4) and then auraptene (1-4) (Fig. 6). The control OHN maintained three hydrogen bonds over the MD simulation period. In contrast, EEE also maintained three hydrogen bonds with LasR over the simulation time and two additional hydrogen bonds until 34 ns. Physcion showed two primary hydrogen bonds with LasR throughout the entire experimental period of

200 ns whereas auraptene showed two strong hydrogen bonds over the whole MD simulation period of 200 ns (Fig 6b). In the case of SarA, EEE showed a high number of hydrogen bonds (1-8), with three strong hydrogen bonds and two moderate hydrogen bonds over the whole MD simulation (Fig. 7e).

3.4.6. Binding free energy analysis

For further insights about the stability of the protein-ligand complex, the MMPBSA binding free energy values were analysed (Table 4). For the LasR protein, the analysis was carried out on the most stable complexes (i.e with epicatechin and OHN). The epicatechin-LasR complex demonstrated a binding energy (ΔE_{Bind}) of -63.717 kJ/mol, whereas the OHN-LasR complex showed a binding energy of -107.223 kJ/mol. Regarding the contribution of active site residues for this energy, it was observed that epicatechin formed strong bonds with Trp60, Thr75, and Arg61 with the values of 9.7056, -3.7003, and -0.4977 kJ/mol, respectively. On the other hand, residues Thr75, Trp60, Asp73, and Arg61 contributed significantly to the binding of OHN with binding energy values of -7.056, 2.066, -0.5164, 0.6377 kJ/mol, respectively (Fig. 8). On the other hand, EEE in complex with SarA showed a binding energy value of -39.899 kJ/mol. This compound interacted with the active site residues Asp188, Glu189 and Arg190 with binding energy values of -1.3837, 9.9308, and 1.536 kJ/mol, respectively (Fig. 9).

3.5. Pharmacokinetic and drug-likeness predictions

Among the ligands displaying the best scores against SarA, 7-*O*-(4-Hydroxy-*E*-cinnamoyl)-spinoside (HCS), 14-dihydroxycard-20(22)-enolide-xylopyranosyl, cyanidin-3,3',5-tri-*O*-β-D-glucopyranoside (CTG), *ent*-epicatechin-(4α→8)-epiafzelechin (2*S*,2'*R*,3*S*,3'*R*,4β form) (EEE)

failed to pass the Lipinski's rule of five (RO5) mainly due to their high molecular weight and/or high logP value [39]. This was also true for the control inhibitor ZINC00990144. On the other hand, all best-scoring ligands against LasR (i.e. physcion, epicatechin, chrysophanol, auraptene) as well as the OHN and eugenol controls presented no violations of the RO5 (Table S8). All the ligands showed positive drug scores with the best value observed for epicatechin (0.87). The drug score is a composite metric derived from various physicochemical parameters and the toxicity of a ligand. A score of 1.0 indicates no risk, 0.8 denotes medium risk, and 0.6 represents high risk [40].

4. DISCUSSION

Many plants are used worldwide in traditional medicine for the treatment of infectious diseases and multiple studies have reported that plant extracts and/or constituents have promising antibiofilm activity against various microorganisms [41-44]. This provides a good rationale for selecting plants as a source of possible new antibiofilm agents [18-19, 45-46]. The screening of plant extracts for the discovery of new antibiofilm agents has to date resulted in the identification of several phytomolecules with promising activity that belong to diverse chemical classes including alkaloids, terpenoids, anthraquinones, and polyphenols. Such antibiofilm compounds, which may also possess antibacterial activity on their own, exert their effects through a range of mechanisms and could serve as useful adjunct therapies to common antibiotic treatments [18, 47]. This would be of particular interest in managing drug-resistant bacterial infections where phytochemicals with antibiofilm activity could synergise the effects of existing antibiotics [48-49].

In the current study, a selection of 20 Bangladeshi plants, used traditionally for infections and/or previously reported to have antibacterial properties, were screened for antibacterial and antibiofilm activity. The tested extracts showed activity to various extents against *S. aureus* and *P. aeruginosa* in agreement with previous reports (Table S1). Although some plants showed similar MICs, they varied greatly in terms of their antibiofilm activity. *C. fistula* showed the highest inhibition of biofilm formation against the pathogens tested and this effect was maintained even at the lowest concentration tested. This species is used extensively in traditional medicine as an effective remedy against infections and its antibacterial activity has previously been demonstrated against several human pathogens including chloramphenicol-resistant *S. aureus* [50-51]. This is the first report of its antibiofilm activity. *A. comosus* is another plant that showed good antibiofilm activity in our study. To the best of our knowledge, there has been only one previous report of its antibiofilm activity against *Porphyromonas gingivalis*, a causative agent of periodontal disease [52].

It has been previously established that the *in vitro* screening of plant extracts followed by *in silico* screening of phytomolecules can help identify potential molecules for advanced studies [53]. Thus, the plant extracts showing the best antibiofilm activity in the present study were further selected for *in silico* screening to investigate which of their constituent(s) may interact with SarA and LasR, two important proteins involved in biofilm formation in *S. aureus* and *P. aeruginosa*, respectively. Our molecular docking study identified a number of phytomolecules with good binding affinity for SarA and LasR. Interestingly, the highest number of phytomolecules showing the best docking scores against SarA and LasR were from *C. fistula*, a plant which demonstrated the best antibiofilm activity in our assay. This suggests that *C. fistula* extract contains a range of antibiofilm natural products that might have contributed to

its observed *in vitro* antibiofilm activity. The molecular docking results identified 14-dihydroxycard-20(22)-enolide-xylopyranosyl, CTG, HCS and EEE as ligands with a high binding affinity for SarA. These compounds interacted with, at least one or more, important residues (i.e. Arg184, Asp188, Glu189 and Arg190) present in the wing region of SarA, which is responsible for DNA binding and activation [12]. Chrysophanol, epicatechin and physcion and auraptene had a high binding affinity for LasR and interacted with important binding site residues (Tyr56, Trp60, Arg61, Asp73, Thr75, Leu110, Ser129) present in the active site of this protein [13, 31]. Detailed molecular interaction analysis revealed several key interactions between physcion and LasR, including hydrogen bonds and hydrophobic contacts, which likely dominate the overall binding (Fig. S2). In addition to this, two unfavourable donor-donor and acceptor-acceptor interactions were found to occur. The significance of these unfavourable interactions or local steric clashes may be compensated by the formation of two hydrogen bonds and several hydrophobic interactions at the binding site. Chrysophanol and physcion belong to the chemical class of anthraquinones. The latter are known for their antibacterial activity [54] and their antibiofilm activity has recently been investigated against methicillin-resistant *S. aureus* with promising results [55-56]. However, neither of these two phytomolecules have previously been investigated for *in vitro* antibiofilm activity. It is interesting to note that a *Rumex japonicus* extract has previously exhibited antibiofilm activity against multidrug-resistant *S. aureus* with chrysophanol and physcion identified among the major components of that extract [57]. Auraptene belongs to the chemical class of coumarins. A series of coumarins were recently investigated for *in vitro* antibiofilm activity against *P. aeruginosa*, where auraptene increased biofilm formation at sub-inhibitory concentration [58]. Further investigations are required to provide conclusive evidence on the effect of coumarins

like auraptene on biofilm formation. Although, it is possible that some antimicrobial compounds may work inversely at subinhibitory concentrations as they could trigger resistance mechanisms in pathogens [27].

MD simulations were further performed to assess the possible conformational changes and stability of each protein-ligand complex. RMSD and RMSF analyses evaluated the stability of the binding of each ligand to its protein target while Rg and SASA analyses indicated the compactness and solvent accessibility of each protein-ligand complex. Hydrogen bonds analyses helped to understand the critical role played by this type of interactions in the stabilisation of ligands within the binding pocket of each protein. Altogether, this evaluated how successfully each ligand could bind to its target in order to induce a biological effect [59]. Epicatechin, followed by auraptene and physcion, exhibited the most stable behaviour and highest number of hydrogen bonds in complex with LasR over the MD simulation period, compared with the other ligands and the control inhibitor OHN. Although the molecular docking results indicated possible donor-donor and acceptor-acceptor unfavorable interactions, the MD results showed that this did not affect the stability of the physcoin-LasR complex. The epicatechin-LasR complex showed the highest compactness and significantly decreased fluctuations of the residues compared to other LasR-ligand complexes. In addition, the epicatechin-LasR exhibited a high binding affinity and interacted strongly with numerous active site residues in the MMPBSA analysis. Epicatechin has previously been reported to increase *P. aeruginosa* biofilm formation at sub-inhibitory concentrations and to display antibiofilm/anti-QS activity against *P. aeruginosa* and other Gram negative bacteria such as *E. coli* and *Chromobacterium violaceum* at higher concentrations [27]. Two of its derivatives, namely catechin and epigallocatechin gallate also inhibited virulence factors production in *P.*

aeruginosa and showed QS inhibitory activity in *P. putida*, respectively [60]. EEE, an epi-afzelechin derivative of epicatechin, complexed with SarA demonstrated a stable profile in the MD analysis along with a high binding energy towards the target protein. Further MMPBSA analysis clarified that EEE interacted with multiple key residues of the DNA binding region of SarA. Overall, the MD simulations revealed that epicatechin and EEE formed the most stable ligand-protein complexes with LasR and SarA proteins, respectively. It is interesting to note that both phytomolecules belong to *C. fistula*, which as aforementioned is an important medicinal plant for infections.

CONCLUSION

The present study provides some support to justify the use of the selected Bangladeshi plants in traditional medicine for the treatment of infectious diseases. Generally speaking, it provides a good example of how existing knowledge on the traditional uses of medicinal plants, combined with *in vitro* and *in silico* screening, can guide the search for new drugs. Further studies are warranted on the most active plants identified in this study as these may prove useful for the discovery of new agents against *S. aureus* and *P. aeruginosa* biofilms. Among the 20 plant extracts tested, *C. fistula* extract exhibited the best antibiofilm activity in the *in vitro* assay. Additionally, epicatechin and EEE, two natural compounds of this plant, were identified as promising ligands against transcriptional regulatory proteins LasR of *P. aeruginosa* and SarA of *S. aureus*, respectively. Further studies are warranted to confirm whether epicatechin and its derivative EEE can be used as model scaffolds for the development of new antibiofilm agents against *P. aeruginosa* and *S. aureus*, respectively.

FUNDING

This research was supported by the Khulna University Research and Innovation Centre (KU/RC-04/2000-281), Khulna, Bangladesh.

CONFLICT OF INTEREST

The authors report no declarations of interest.

ACKNOWLEDGEMENT

M Khairuzzaman thanks Khulna University for the provision of postgraduate research funding.

SUPPLEMENTARY MATERIAL

Supplementary file.

References:

1. Flemming, H.-C.; Wingender, J., The biofilm matrix. *Nat. Rev. Microbiol.* **2010,** *8* (9), 623-633. https://doi.org/10.1038/nrmicro2415
2. van Loosdrecht, M. C. M.; Eikelboom, D.; Gjaltema, A.; Mulder, A.; Tijhuis, L.; Heijnen, J. J., Biofilm structures. *Water Sci. Technol.* **1995,** *32* (8), 35-43. https://doi.org/https://doi.org/10.1016/0273-1223(96)00005-4
3. Rabin, N.; Zheng, Y.; Opoku-Temeng, C.; Du, Y.; Bonsu, E.; Sintim, H. O., Biofilm formation mechanisms and targets for developing antibiofilm agents. *Future Med. Chem.* **2015,** *7* (4), 493-512. https://doi.org/10.4155/fmc.15.6
4. Watnick, P.; Kolter, R., Biofilm, city of microbes. *Journal of Bacteriology* **2000,** *182* (10), 2675-2679. https://doi.org/doi:10.1128/JB.182.10.2675-2679.2000
5. Shakib, P.; Saki, R.; Marzban, A.; Goudarzi, G.; Ghotekar, S.; Cheraghipour, K.; Zolfaghari Reza, M., Antibacterial effects of nanocomposites on efflux pump expression and biofilm production in *Pseudomonas aeruginosa*: A Systematic Review. *Curr. Pharm. Biotechnol.* **2024,** *25* (1), 77-92. https://doi.org/http://dx.doi.org/10.2174/1389201024666230428121122

6. Hoffman, L. R.; D'Argenio, D. A.; MacCoss, M. J.; Zhang, Z.; Jones, R. A.; Miller, S. I., Aminoglycoside antibiotics induce bacterial biofilm formation. *Nature* **2005,** *436* (7054), 1171-1175. https://doi.org/10.1038/nature03912
7. Linares, J. F.; Gustafsson, I.; Baquero, F.; Martinez, J. L., Antibiotics as intermicrobial signaling agents instead of weapons. *Proc. Natl. Acad. Sci.* **2006,** *103* (51), 19484-9. https://doi.org/10.1073/pnas.0608949103
8. Costerton, J. W.; Stewart, P. S.; Greenberg, E. P., Bacterial biofilms: a common cause of persistent infections. *Science* **1999,** *284* (5418), 1318-22. https://doi.org/10.1126/science.284.5418.1318
9. Li, X.-H.; Lee, J.-H., Antibiofilm agents: A new perspective for antimicrobial strategy. *J. Microbiol.* **2017,** *55* (10), 753-766. https://doi.org/10.1007/s12275-017-7274-x
10. Lewis, K., Riddle of biofilm resistance. *Antimicrob. Agents Chemother.* **2001,** *45* (4), 999-1007. https://doi.org/doi:10.1128/AAC.45.4.999-1007.2001
11. Khan, S. A. M.; Lee, J., Novel strategies for combating pathogenic biofilms using plant products and microbial antibiosis. *Curr. Pharm. Biotechnol.* **2016,** *17* (2), 126-140. https://doi.org/http://dx.doi.org/10.2174/1389201016666150907113228
12. Liu, Y.; Manna, A. C.; Pan, C.-H.; Kriksunov, I. A.; Thiel, D. J.; Cheung, A. L.; Zhang, G., Structural and function analyses of the global regulatory protein SarA from *Staphylococcus aureus*. *Proc. Natl. Acad. Sci.* **2006,** *103* (7), 2392-2397.
13. Bottomley, M. J.; Muraglia, E.; Bazzo, R.; Carfì, A., Molecular insights into quorum sensing in the human pathogen *Pseudomonas aeruginosa* from the structure of the virulence regulator LasR bound to its autoinducer. *J. Biol. Chem.* **2007,** *282* (18), 13592-13600. https://doi.org/10.1074/jbc.M700556200
14. Roberts, C.; Anderson, K. L.; Murphy, E.; Projan, S. J.; Mounts, W.; Hurlburt, B.; Smeltzer, M.; Overbeek, R.; Disz, T.; Dunman, P. M., Characterizing the effect of the *Staphylococcus aureus* virulence factor regulator, SarA, on log-phase mRNA half-lives. *J. Bacteriol.* **2006,** *188* (7), 2593-603. https://doi.org/10.1128/jb.188.7.2593-2603.2006
15. Rechtin, T. M.; Gillaspy, A. F.; Schumacher, M. A.; Brennan, R. G.; Smeltzer, M. S.; Hurlburt, B. K., Characterization of the SarA virulence gene regulator of *Staphylococcus aureus*. *Mol. Microbiol.* **1999,** *33* (2), 307-316. https://doi.org/https://doi.org/10.1046/j.1365-2958.1999.01474.x
16. Heurlier, K.; Dénervaud, V.; Haas, D., Impact of quorum sensing on fitness of *Pseudomonas aeruginosa*. *Int. J. Med. Microbiol.* **2006,** *296* (2), 93-102. https://doi.org/https://doi.org/10.1016/j.ijmm.2006.01.043
17. Lee, J.; Zhang, L., The hierarchy quorum sensing network in *Pseudomonas aeruginosa*. *Protein Cell* **2015,** *6* (1), 26-41. https://doi.org/10.1007/s13238-014-0100-x
18. Song, X.; Xia, Y.-X.; He, Z.-D.; Zhang, H.-J., A review of natural products with anti-biofilm activity. *Curr. Org. Chem.* **2018,** *22* (8), 789-817. https://doi.org/http://dx.doi.org/10.2174/1385272821666170620110041
19. Lu, L.; Hu, W.; Tian, Z.; Yuan, D.; Yi, G.; Zhou, Y.; Cheng, Q.; Zhu, J.; Li, M., Developing natural products as potential anti-biofilm agents. *Chin. Med.* **2019,** *14* (1), 11. https://doi.org/10.1186/s13020-019-0232-2
20. Siddique, H.; Pendry, B.; Rashid, M. A.; Rahman, M. M., Medicinal plants used to treat infectious diseases in the central part and a northern district of Bangladesh – An

ethnopharmacological perception. *J. Herb. Med.* **2021,** *29*, 100484. https://doi.org/https://doi.org/10.1016/j.hermed.2021.100484

21. Heinrich, M., Ethnobotany and its role in drug development. *Phytother. Res.* **2000,** *14* (7), 479-488. https://doi.org/https://doi.org/10.1002/1099-1573(200011)14:7

22. Islam, M. K.; Saha, S.; Mahmud, I.; Mohamad, K.; Awang, K.; Jamal Uddin, S.; Rahman, M. M.; Shilpi, J. A., An ethnobotanical study of medicinal plants used by tribal and native people of Madhupur forest area, Bangladesh. *J. Ethnopharmacol.* **2014,** *151* (2), 921-30. https://doi.org/10.1016/j.jep.2013.11.056

23. Wiegand, I.; Hilpert, K.; Hancock, R. E. W., Agar and broth dilution methods to determine the minimal inhibitory concentration (MIC) of antimicrobial substances. *Nat. Protoc.* **2008,** *3* (2), 163-175. https://doi.org/10.1038/nprot.2007.521

24. Zihad, S.; Hasan, M. T.; Sultana, M. S.; Nath, S.; Nahar, L.; Rashid, M. A.; Uddin, S. J.; Sarker, S. D.; Shilpi, J. A., Isolation and characterization of antibacterial compounds from *Aspergillus fumigatus*: An endophytic fungus from a mangrove plant of the Sundarbans. *Evid. Based Complement. Alternat. Med.* **2022,** *2022*, 9600079. https://doi.org/10.1155/2022/9600079

25. O'Toole, G. A., Microtiter dish biofilm formation assay. *J. Vis. Exp.* **2011,** *47*, 2437. https://doi.org/10.3791/2437

26. Zia, G.; Sadia, H.; Nazir, S.; Ejaz, K.; Ali, S.; Ihsan ul, H.; Iqbal, T.; Khan, A. R. M.; Raza, A.; Andleeb, S., In vitro studies on cytotoxic, DNA protecting, antibiofilm and antibacterial effects of biogenic silver nanoparticles prepared with *Bergenia ciliata* rhizome extract. *Curr. Pharm. Biotechnol.* **2018,** *19* (1), 68-78. https://doi.org/http://dx.doi.org/10.2174/1389201019666180417160049

27. Plyuta, V.; Zaitseva, J.; Lobakova, E.; Zagoskina, N.; Kuznetsov, A.; Khmel, I., Effect of plant phenolic compounds on biofilm formation by *Pseudomonas aeruginosa*. *APMIS Journal* **2013,** *121* (11), 1073-1081. https://doi.org/https://doi.org/10.1111/apm.12083

28. Olszewska, M. A.; Gędas, A.; Simões, M., The effects of eugenol, trans-cinnamaldehyde, citronellol, and terpineol on *Escherichia coli* biofilm control as assessed by culture-dependent and -independent methods. *Molecules* **2020,** *25* (11). https://doi.org/10.3390/molecules25112641

29. Arya, R.; Ravikumar, R.; Santhosh, R. S.; Princy, S. A., SarA based novel therapeutic candidate against *Staphylococcus aureus* associated with vascular graft infections. *Front. Microbiol.* **2015,** *6*, 416. https://doi.org/10.3389/fmicb.2015.00416

30. Yu, J.; Jiang, F.; Zhang, F.; Pan, Y.; Wang, J.; Han, P.; Tang, J.; Shen, H., Virtual screening for novel SarA inhibitors to prevent biofilm formation of *Staphylococcus aureus* in prosthetic joint infections. *Front. Microbiol.* **2020,** *11*. https://doi.org/10.3389/fmicb.2020.587175

31. Liu, G.-Y.; Guo, B.-Q.; Chen, W.-N.; Cheng, C.; Zhang, Q.-L.; Dai, M.-B.; Sun, J.-R.; Sun, P.-H.; Chen, W.-M., Synthesis, molecular docking, and biofilm formation inhibitory activity of 5-substituted 3,4-dihalo-5H-furan-2-one derivatives on *Pseudomonas aeruginosa*. *Chem. Biol. Drug Des.* **2012,** *79* (5), 628-638. https://doi.org/https://doi.org/10.1111/j.1747-0285.2012.01342.x

32. Trott, O.; Olson, A. J., AutoDock Vina: improving the speed and accuracy of docking with a new scoring function, efficient optimization, and multithreading. *J. Comput. Chem.* **2010,** *31* (2), 455-61. https://doi.org/10.1002/jcc.21334

33. Dallakyan, S.; Olson, A. J., Small-Molecule Library Screening by Docking with PyRx. In *Chemical Biology: Methods and Protocols*, Hempel, J. E.; Williams, C. H.; Hong, C. C., Eds. Springer New York: New York, NY, 2015; pp 243-250.
34. Abraham, M. J.; Murtola, T.; Schulz, R.; Páll, S.; Smith, J. C.; Hess, B.; Lindahl, E., GROMACS: High performance molecular simulations through multi-level parallelism from laptops to supercomputers. *SoftwareX* **2015,** *1-2*, 19-25. https://doi.org/https://doi.org/10.1016/j.softx.2015.06.001
35. Huang, J.; Rauscher, S.; Nawrocki, G.; Ran, T.; Feig, M.; de Groot, B. L.; Grubmüller, H.; MacKerell, A. D., CHARMM36m: an improved force field for folded and intrinsically disordered proteins. *Nat. Methods* **2017,** *14* (1), 71-73. https://doi.org/10.1038/nmeth.4067
36. Vanommeslaeghe, K.; Hatcher, E.; Acharya, C.; Kundu, S.; Zhong, S.; Shim, J.; Darian, E.; Guvench, O.; Lopes, P.; Vorobyov, I.; Mackerell, A. D., Jr., CHARMM general force field: A force field for drug-like molecules compatible with the CHARMM all-atom additive biological force fields. *J. Comput. Chem.* **2010,** *31* (4), 671-90. https://doi.org/10.1002/jcc.21367
37. Kumari, R.; Kumar, R.; Lynn, A., g_mmpbsa—A GROMACS Tool for high-throughput MM-PBSA calculations. *J. Chem. Inf. Model.* **2014,** *54* (7), 1951-1962. https://doi.org/10.1021/ci500020m
38. Daina, A.; Michielin, O.; Zoete, V., SwissADME: a free web tool to evaluate pharmacokinetics, drug-likeness and medicinal chemistry friendliness of small molecules. *Sci. Rep.* **2017,** *7* (1), 42717. https://doi.org/10.1038/srep42717
39. Lipinski, C. A.; Lombardo, F.; Dominy, B. W.; Feeney, P. J., Experimental and computational approaches to estimate solubility and permeability in drug discovery and development settings. *Adv. Drug Deliv Rev.* **2001,** *46* (1), 3-26. https://doi.org/https://doi.org/10.1016/S0169-409X(00)00129-0
40. Messali, M.; Aouad, M. R.; El-Sayed, W. S.; Ali, A. A.; Ben Hadda, T.; Hammouti, B., New eco-friendly 1-alkyl-3-(4-phenoxybutyl) imidazolium-based ionic liquids derivatives: a green ultrasound-assisted synthesis, characterization, antibacterial activity and POM analyses. *Molecules* **2014,** *19* (8), 11741-59. https://doi.org/10.3390/molecules190811741
41. Budri, P. E.; Silva, N. C. C.; Bonsaglia, E. C. R.; Fernandes, A.; Araújo, J. P.; Doyama, J. T.; Gonçalves, J. L.; Santos, M. V.; Fitzgerald-Hughes, D.; Rall, V. L. M., Effect of essential oils of *Syzygium aromaticum* and *Cinnamomum zeylanicum* and their major components on biofilm production in *Staphylococcus aureus* strains isolated from milk of cows with mastitis. *J. Dairy Sci.* **2015,** *98* (9), 5899-5904. https://doi.org/https://doi.org/10.3168/jds.2015-9442
42. Bazargani, M. M.; Rohloff, J., Antibiofilm activity of essential oils and plant extracts against *Staphylococcus aureus* and *Escherichia coli* biofilms. *Food Control* **2016,** *61*, 156-164. https://doi.org/https://doi.org/10.1016/j.foodcont.2015.09.036
43. Bakkiyaraj, D.; Nandhini, J. R.; Malathy, B.; Pandian, S. K., The anti-biofilm potential of pomegranate (*Punica granatum* L.) extract against human bacterial and fungal pathogens. *Biofouling* **2013,** *29* (8), 929-937. https://doi.org/10.1080/08927014.2013.820825
44. Caesar, L. K.; Cech, N. B., Synergy and antagonism in natural product extracts: when 1 + 1 does not equal 2. *Nat. Prod. Rep.* **2019,** *36* (6), 869-888. https://doi.org/10.1039/c9np00011a

45. Woo, S. G.; Lee, S. Y.; Lee, S. M.; Lim, K. H.; Ha, E. J.; Eom, Y. B., Activity of novel inhibitors of *Staphylococcus aureus* biofilms. *Folia Microbiol.* **2017,** *62* (2), 157-167. https://doi.org/10.1007/s12223-016-0485-4

46. Kolouchová, I.; Maťátková, O.; Paldrychová, M.; Kodeš, Z.; Kvasničková, E.; Sigler, K.; Čejková, A.; Šmidrkal, J.; Demnerová, K.; Masák, J., Resveratrol, pterostilbene, and baicalein: plant-derived anti-biofilm agents. *Folia Microbiol.* **2018,** *63* (3), 261-272. https://doi.org/10.1007/s12223-017-0549-0

47. Mishra, R.; Panda, A. K.; De Mandal, S.; Shakeel, M.; Bisht, S. S.; Khan, J., Natural anti-biofilm agents: strategies to control biofilm-forming pathogens. *Front. Microbiol.* **2020,** *11*. https://doi.org/10.3389/fmicb.2020.566325

48. Rosato, A.; Sblano, S.; Salvagno, L.; Carocci, A.; Clodoveo, M. L.; Corbo, F.; Fracchiolla, G., Anti-biofilm inhibitory synergistic effects of combinations of essential oils and antibiotics. *Antibiotics* **2020,** *9* (10). https://doi.org/10.3390/antibiotics9100637

49. Yang, Y.; Zhang, Z.; Li, S.; Ye, X.; Li, X.; He, K., Synergy effects of herb extracts: Pharmacokinetics and pharmacodynamic basis. *Fitoterapia* **2014,** *92*, 133-147. https://doi.org/https://doi.org/10.1016/j.fitote.2013.10.010

50. Duraipandiyan, V.; Ignacimuthu, S., Antibacterial and antifungal activity of *Cassia fistula* L.: An ethnomedicinal plant. *J. Ethnopharmacol.* **2007,** *112* (3), 590-594. https://doi.org/https://doi.org/10.1016/j.jep.2007.04.008

51. Mwangi, R. W.; Macharia, J. M.; Wagara, I. N.; Bence, R. L., The medicinal properties of *Cassia fistula* L: A review. *Biomed. Pharmacother.* **2021,** *144*, 112240. https://doi.org/https://doi.org/10.1016/j.biopha.2021.112240

52. Gani Soulissa, A.; Lombardo, B.; Sari Widyarman, A., Antibacterial and antibiofilm efficacy of pineapple hump (*Ananas comosus*) on *Porphyromonas gingivalis* in vitro. *J. Dent. Indones.* **2021,** *28 (3)*, 153-157. 10.14693/jdi.v28i3.1267

53. Gupta, M.; Sharma, R.; Kumar, A., Docking techniques in pharmacology: How much promising? *Comput. Biol. Chem.* **2018,** *76*, 210-217. https://doi.org/https://doi.org/10.1016/j.compbiolchem.2018.06.005

54. Qun, T.; Zhou, T.; Hao, J.; Wang, C.; Zhang, K.; Xu, J.; Wang, X.; Zhou, W., Antibacterial activities of anthraquinones: structure–activity relationships and action mechanisms. *RSC Med. Chem.* **2023,** *14* (8), 1446-1471. https://doi.org/10.1039/D3MD00116D

55. Song, Z.-M.; Zhang, J.-L.; Zhou, K.; Yue, L.-M.; Zhang, Y.; Wang, C.-Y.; Wang, K.-L.; Xu, Y., Anthraquinones as potential antibiofilm agents against methicillin-resistant *Staphylococcus aureus*. *Front. Microbiol.* **2021,** *12*. https://doi.org/10.3389/fmicb.2021.709826

56. Farooq, U.; Khan, S.; Naz, S.; Khan, A.; Khan, A.; Ahmed, A.; Rauf, A.; Bukhari, S. M.; Khan, S. A.; Kamil, A.; Riaz, N.; Khan, A. R., Three new anthraquinone derivatives isolated from *Symplocos racemosa* and their antibiofilm activity. *Chinese J. Nat. Med.* **2017,** *15* (12), 944-949. https://doi.org/https://doi.org/10.1016/S1875-5364(18)30011-6

57. Kim, G.; Xu, Y. J.; Farha, A. K.; Sui, Z. Q.; Corke, H., Bactericidal and antibiofilm properties of Rumex japonicus Houtt. on multidrug-resistant *Staphylococcus aureus* isolated from milk. *J. Dairy Sci.* **2022,** *105* (3), 2011-2024. https://doi.org/https://doi.org/10.3168/jds.2021-21221

58. Tajani, A. S.; Amiri Tehranizadeh, Z.; Pourmohammad, A.; Pourmohammad, A.; Iranshahi, M.; Farhadi, F.; Soheili, V.; Fazly Bazzaz, B. S., Anti-quorum sensing and antibiofilm activity of coumarin derivatives against *Pseudomonas aeruginosa* PAO1: Insights from in vitro and in silico studies. *Iran. J. Basic Med. Sci.* **2023,** *26* (4), 445-452. https://doi.org/10.22038/ijbms.2023.69016.15047

59. Durrant, J. D.; McCammon, J. A., Molecular dynamics simulations and drug discovery. *BMC Biol.* **2011,** *9* (1), 71. https://doi.org/10.1186/1741-7007-9-71

60. Ta, C. A.; Arnason, J. T., Mini review of phytochemicals and plant taxa with activity as microbial biofilm and quorum sensing inhibitors. *Molecules* **2015,** *21* (1), E29. https://doi.org/10.3390/molecules21010029

Table 1: MIC values of the studied plant extracts against *S. aureus* and *P. aeruginosa*.

Plant name	Part used for extraction	Yield (%)	MIC (µg/mL)	
			S. aureus	*P. aeruginosa*
Amaranthus spinosus L.	Whole plant	1.84	250	62.5
Amaranthus blitum L.	Whole plant	0.55	500	500
Ananas comosus (L.) Merr.	Fruits	7.84	500	250
Calotropis gigantea (L.) Dryand.	Leaves	1.49	250	500
Capsicum frutescens L.	Fruits	0.47	500	500
Carica papaya L.	Leaves	1.46	500	500
Cassia fistula L.	Leaves	3.23	500	500
Centella asiatica (L.) Urb.	Whole plant	2.69	500	500
Chenopodium album Bosc ex Moq.	Whole plant	0.66	250	250
Citrus maxima (Burm.) Merr.	Fruit peels	1.17	500	500
Coccinia grandis (L.) Voigt	Whole plant	1.77	500	500
Feronia limonia Swingle	Leaves	0.83	250	500
Ficus benghalensis L.	Leaves	0.22	500	500
Hibiscus rosa-sinensis L.	Leaves	1.39	500	500
Justicia adhatoda L.	Leaves	0.66	250	62.5
Mangifera indica L.	Stem bark	11.58	500	500

Monoon longifolium (Sonn.) B.Xue & R.M.K.Saunders	Leaves	1.99	62.5	125
Tamarindus indica L.	Leaves	1.49	250	250
Terminalia chebula Retz.	Fruits	11.67	500	500
Vitex negundo L.	Leaves	8.02	500	250
Ciprofloxacin	-	-	1.56	1.56
Gentamicin	-	-	0.78	0.78
Eugenol	-	-	>25	>25
Epicatechin	-	-	>25	>25

656

657

658

659

660 **Table 2: Predicted free binding energy (docking score ΔG in kcal/mol) of *A. comosus, A.***

661 ***spinosus, C. fistula, T. indica* phytoconstituents and control ligands towards SarA**

662

Origin	Ligand	Docking score
A. comosus	Cyanidin-3,3',5-tri-*O*-β-D-glucopyranoside (**CTG**)	-7.6
	Ergosterol peroxide	-7.0
A. spinosus	Oleanolic acid-3-*O*-[β-D-Glucopyranosyl-(1→4)-β-D-glucopyranosyl-(1→4)-β-D-glucuronopyranoside]	-7.3
	7-*O*-(4-Hydroxy-*E*-cinnamoyl)-spinoside (**HCS**)	-7.7
C. fistula	Cassiaflavan-(4β→6)-epiafzelechin, (2*S*,2'*R*,3'*R*,4α form)	-7.1
	Cassiaflavan-(4α→6)-epiafzelechin (2*S*,2'*R*,3'*R*,4β form)	-7.1
	ent-Epicatechin-(4α→8)-epiafzelechin (2*S*,2'*R*,3*S*,3'*R*,4β form) (**EEE**)	-7.6
	Epicatechin-(4β→8)-*ent*-epiafzelechin (2*R*,2'*S*,3*R*,3'*S*,4α form)	-7.3
T. indica	14-Dihydroxycard-20(22)-enolide-xylopyranosyl	-7.7
Control	ZINC00990144	-7.9
	SarABI	-5.8
	Eugenol	-4.8

663

664

665

666

667

668

669

670

671

672

673

674

675

676 **Table 3: Predicted free binding energy (docking score ΔG in kcal/mol) of *A. comosus, A.***

677 ***spinosus, C. fistula, F. limonia* phytoconstituents and control ligands towards LasR**

Origin	Ligand	Docking score
A. comosus	Ananasate	-9.8
	Chrysoeriol	-10.0
A. spinosus	Amaricin	-9.9
	Quercetin	-10.4
C. fistula	4-Hydroxy-5-methoxyanthraquinone-2-carboxaldehyde	-9.9
	3,4,4',7,8-Pentahydroxyflavan (2ξ,3ξ,4ξ form)	-9.8
	Chrysophanol	-10.5
	Epicatechin	-10.5
	Physcion	-11.0
F. limonia	Auraptene	-10.8
	N-3-oxo dodecanoyl-L homoserin lactone (OHN)	-9.0
Control	Eugenol	-6.8

678

679

680

681

682

683

684

685

686

687

688

689

690

691

692

693

694 **Table 4: Predicted MMPBSA binding free energy analysis.**

Ligand	Energy terms (kJ/mol)				
	$\Delta E_{\text{Van der Waal}}$	$\Delta E_{\text{Electrostatic}}$	$\Delta E_{\text{Solvation; Polar}}$	$\Delta E_{\text{Solvation; SASA}}$	ΔE_{Bind}
Epicatechin-LasR	-158.753 ± 9.965	-29.031 ± 8.700	140.763 ± 19.098	-16.698 ± 0.723	-63.717 ± 12.610
OHN-LasR	-182.464 ± 10.909	-84.845 ± 11.308	180.809 ± 13.049	-20.723 ± 0.698	-107.223 ± 1.749
EEE- SarA	-133.144 ± 15.870	-89.621 ± 29.099	201.125 ± 29.886	-18.260 ± 1.380	-39.899 ± 17.917

695

696

697

698

699

700

701

702

703

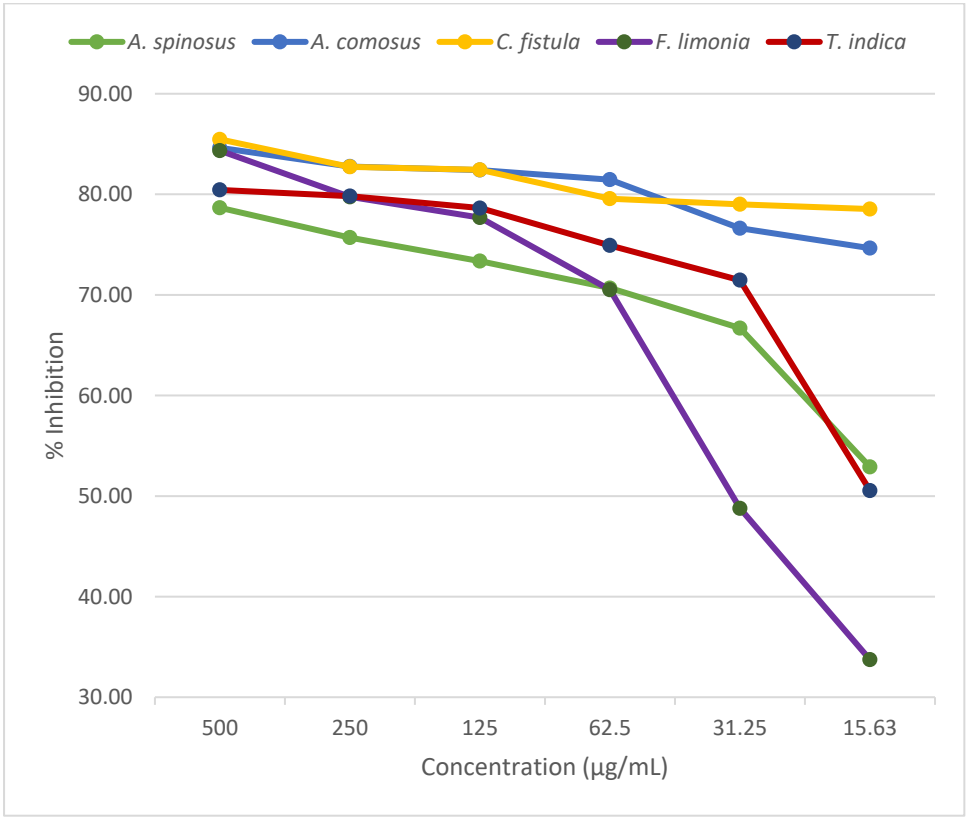

Fig. 1: % Inhibition of *S. aureus* biofilm formation by the best performing five plant extracts.

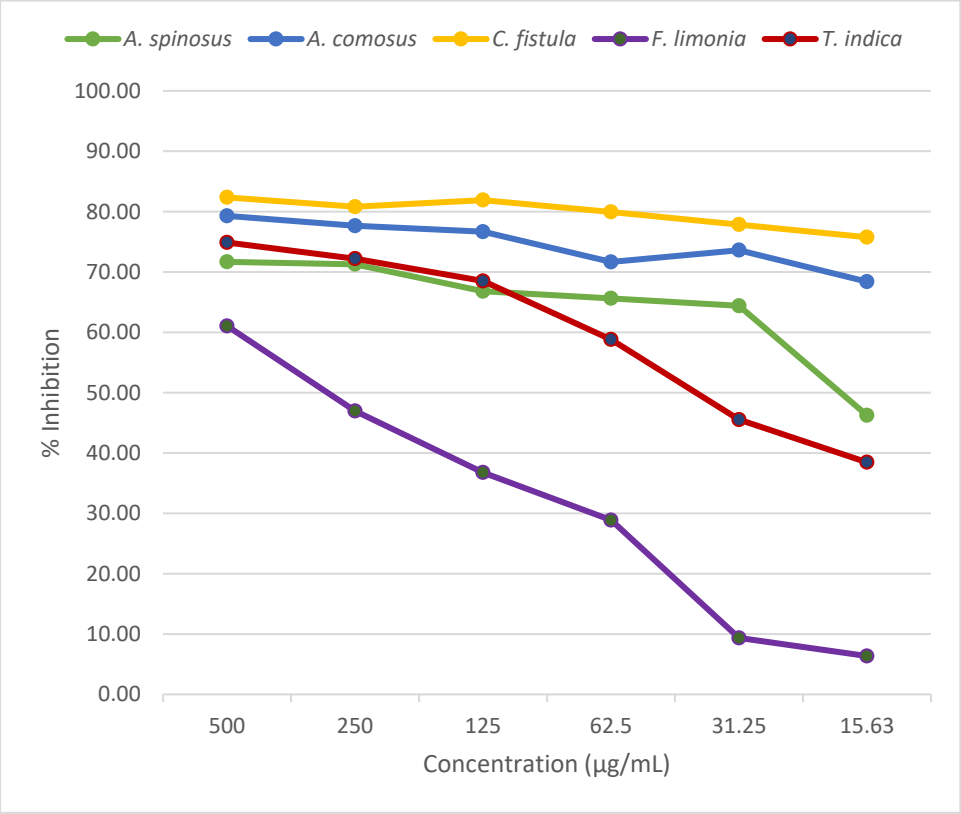

730

731 **Fig. 2: % Inhibition of *P. aeruginosa* biofilm formation by the best performing five plant**
732 **extracts.**
733
734
735
736
737
738
739
740
741
742

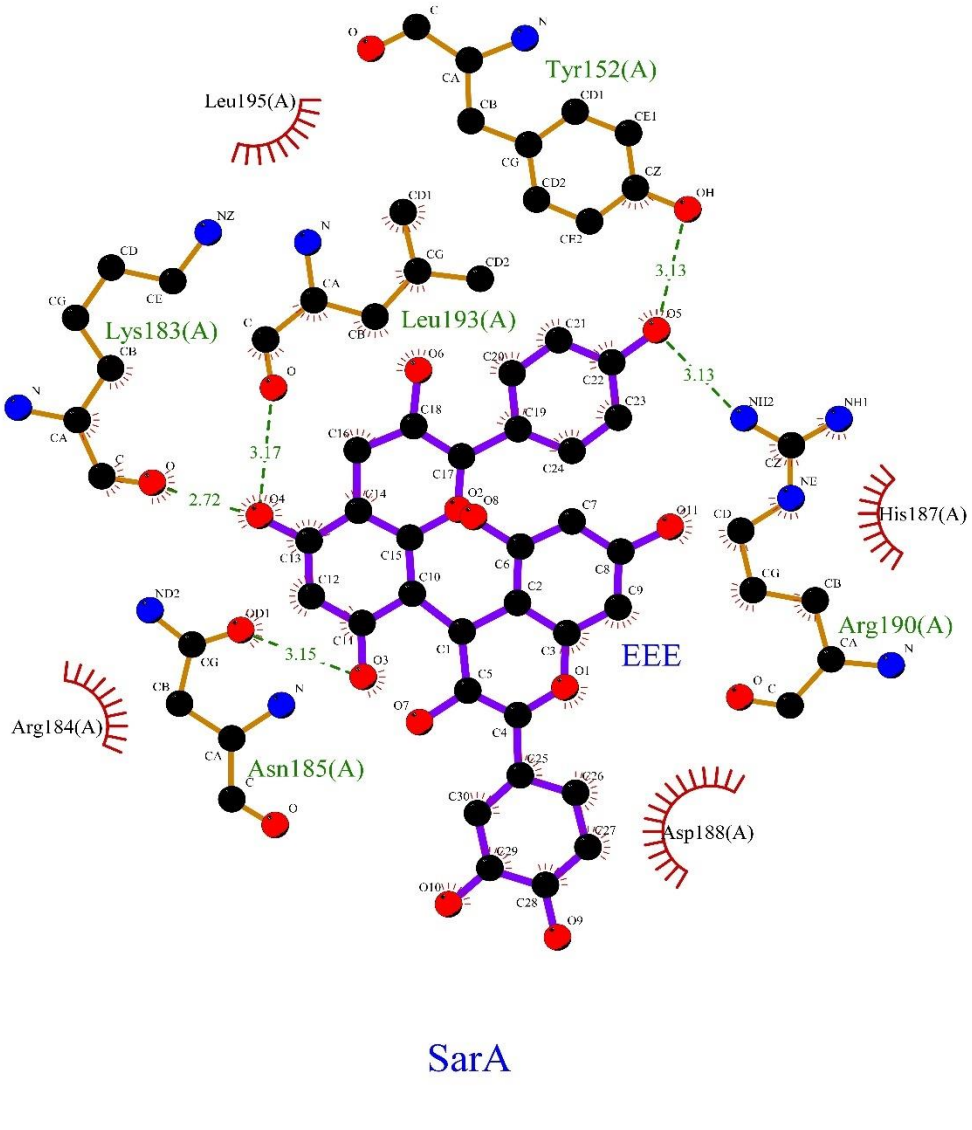

Fig. 3: Docked pose of *ent*-epicatechin-(4*α*→8)-epiafzelechin (2*S*,2'*R*,3*S*,3'*R*,4β form) in the binding site of *S. aureus* SarA, showing hydrogen bonds with key amino acid residues. Bond distances are in angstrom.

750

751

752

753

754

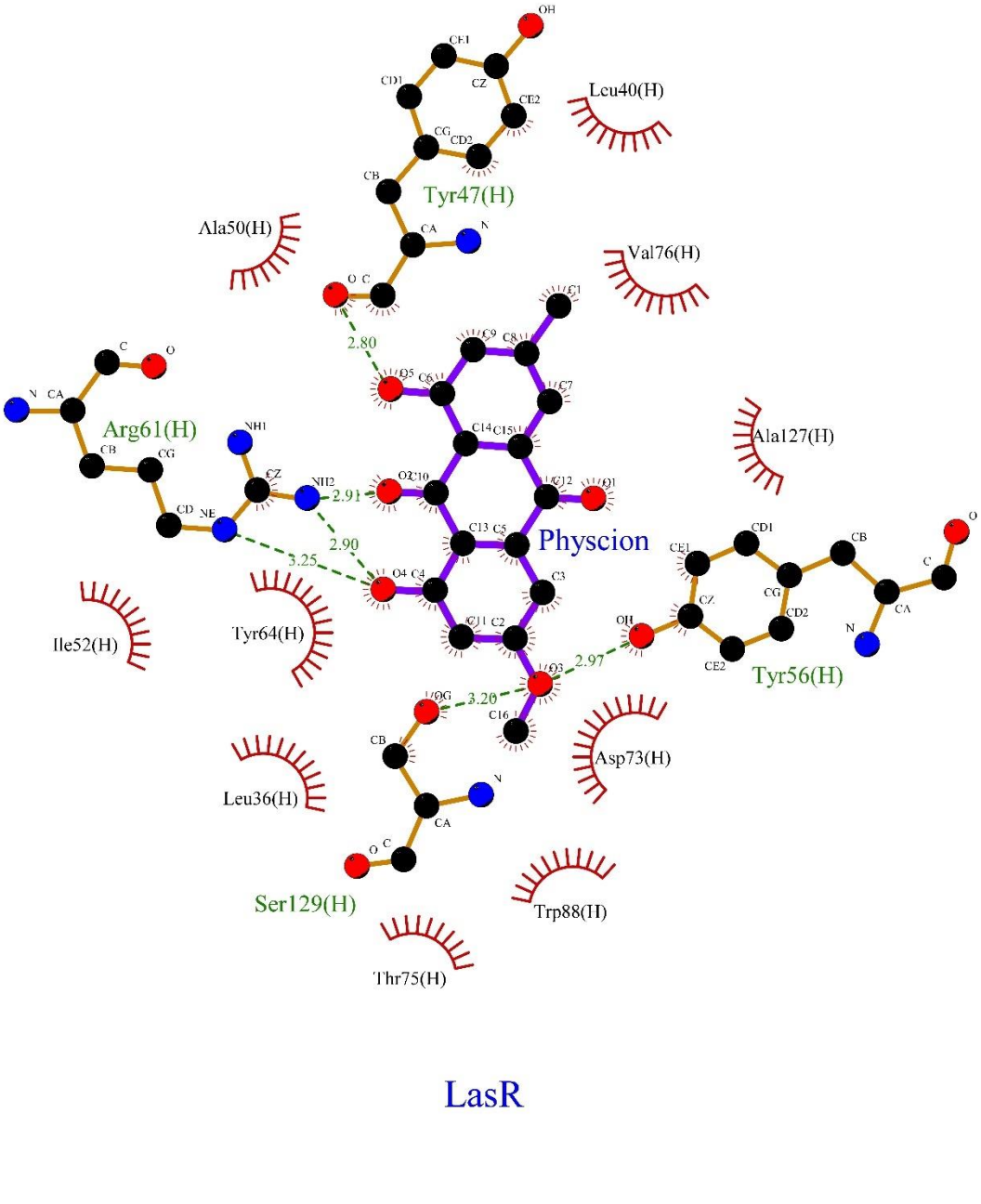

Fig. 4: Docked pose of physcion in the binding site of *P. aeruginosa* LasR, showing hydrogen bonds with key amino acid residues. Bond distances are in angstrom.

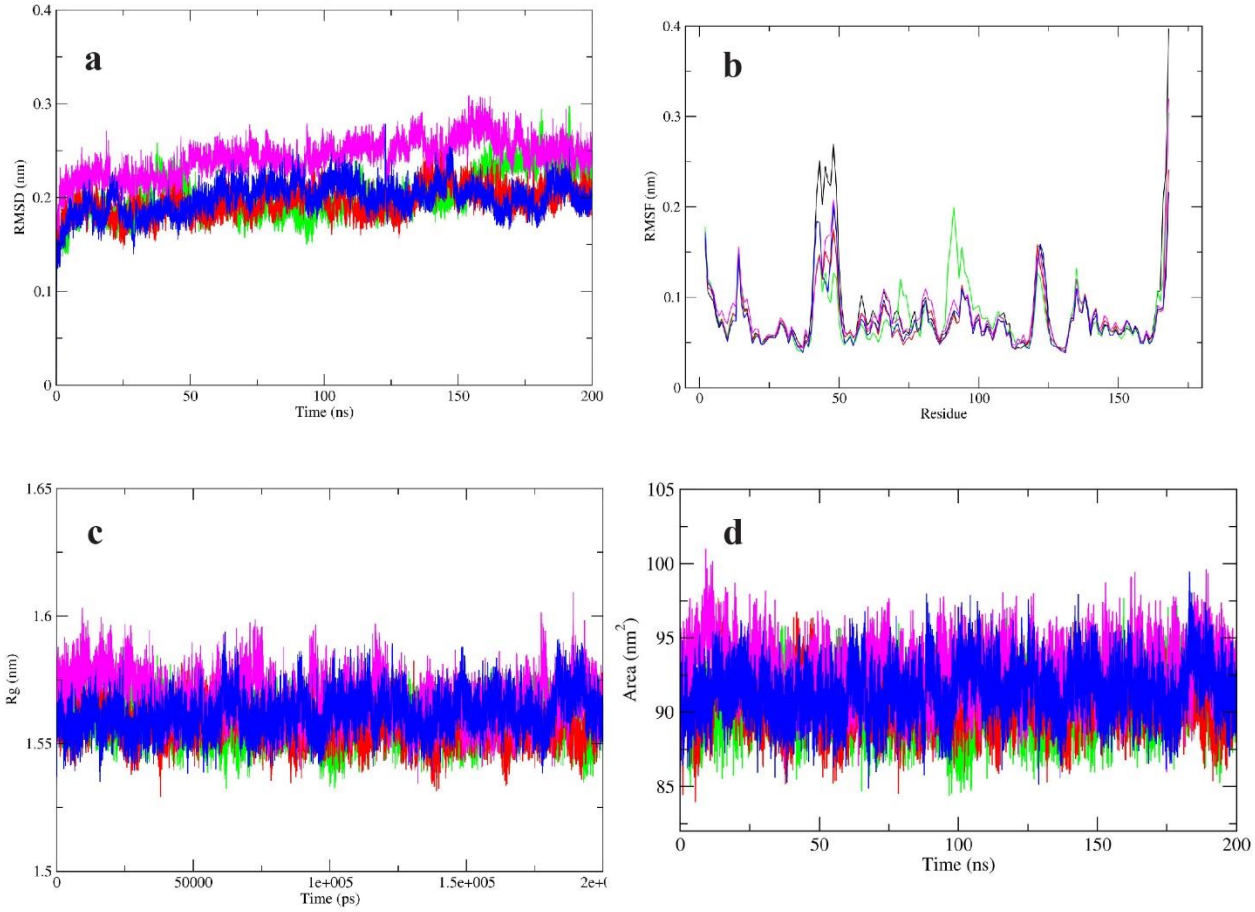

Fig. 5: Plot of a) RMSD, b) RMSF c) Rg, and d) SASA of apo protein (black) and physcion (green), epicatechin (blue), auraptene (magenta) and *N*-3-oxo dodecanoyl-L homoserine lactone (red) in complex with *P. aeruginosa* LasR

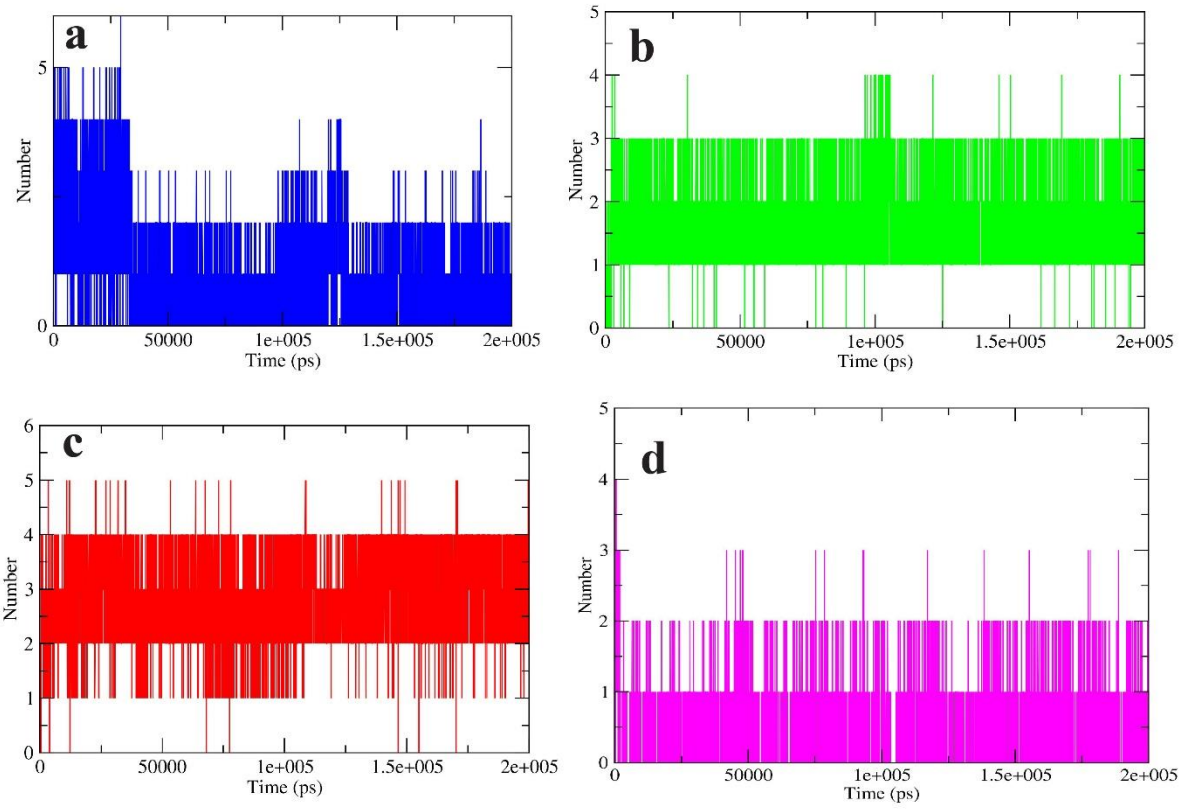

Fig. 6: Hydrogen bond plot of a) epicatechin, b) physcion, c) OHN, and d) auraptene in complex with *P. aeruginosa* LasR

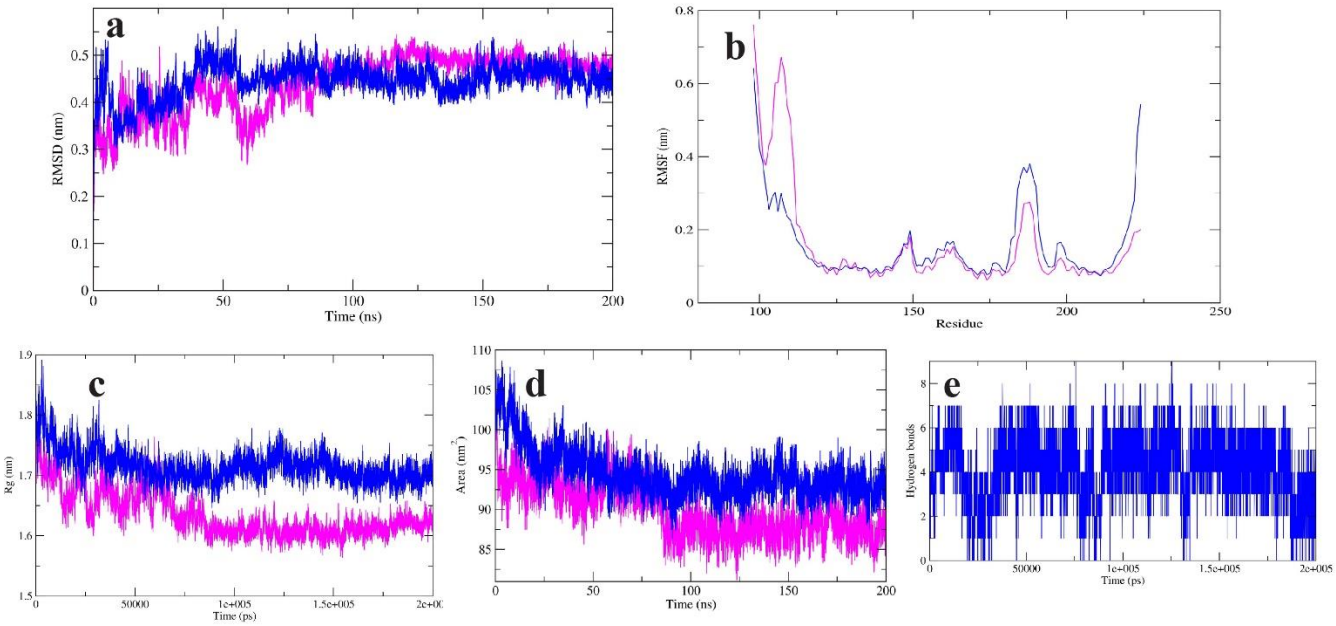

Fig. 7: Plot of a) RMSD, b) RMSF c) Rg, and d) SASA of EEE-SarA complex (blue) and apo protein of *S. aureus* SarA (magenta). e) Hydrogen bond plot of EEE in complex with *S. aureus* SarA.

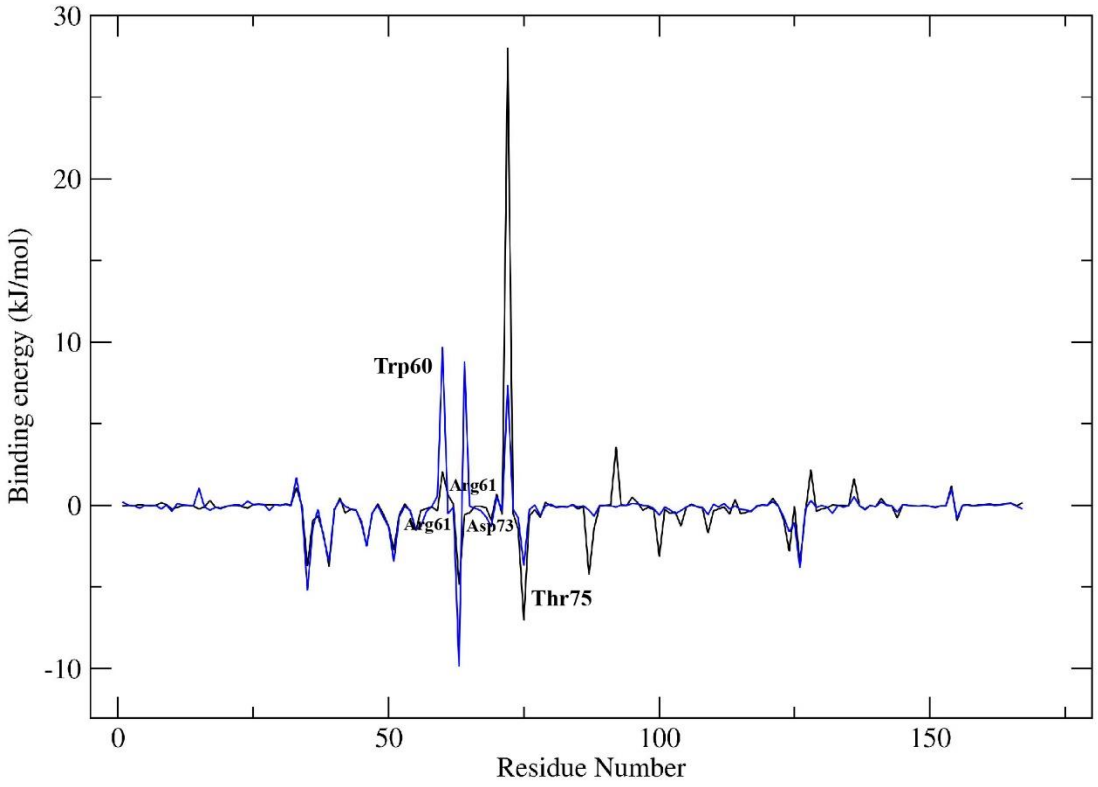

Fig. 8: Plot of MMPBSA analysis of LasR in complex with epicatechin (blue), and OHN (black).

819

820

821

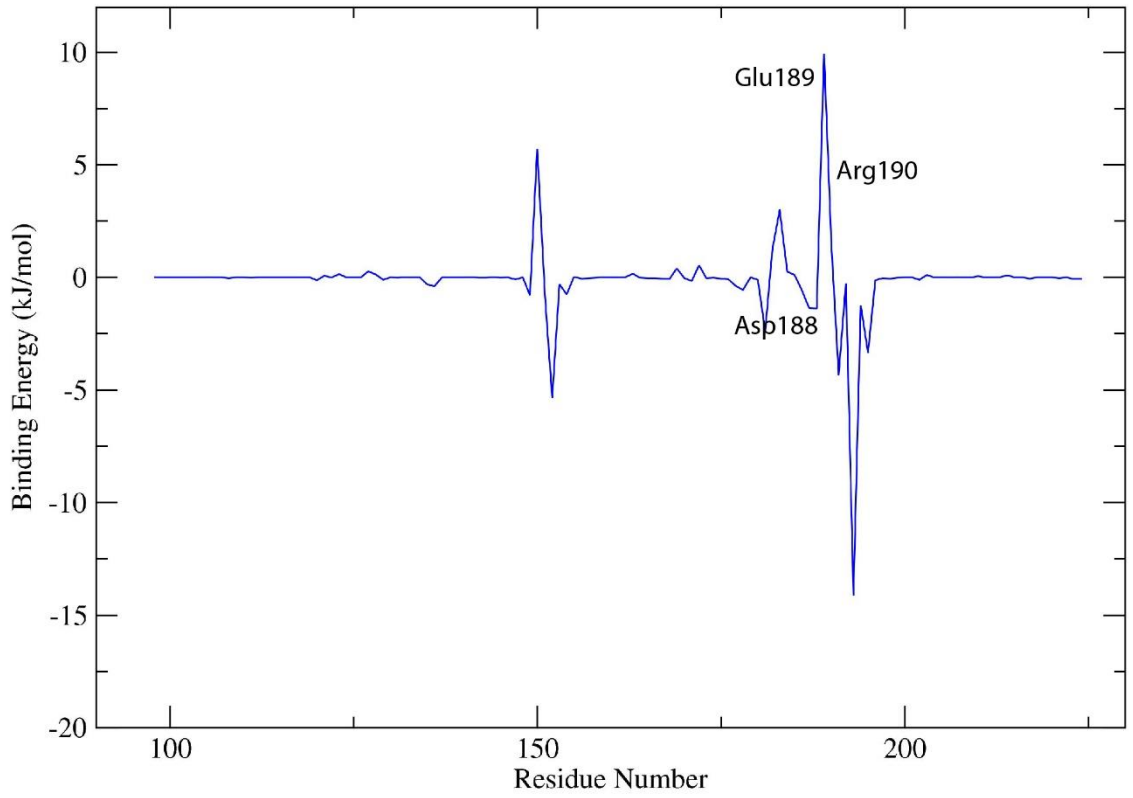

822

823 **Fig. 9: Plot of MMPBSA analysis of SarA in complex with EEE.**

824

825

826

827

828

829